# Supporting Information

# Probing the Reactivity of Pt/Ceria Nanocatalysts towards Methanol Oxidation: From Ionic Single-Atom Sites to Metallic Nanoparticles

Nguyen-Dung Tran, Matteo Farnesi Camellone, and Stefano Fabris[*]

*CNR-IOM DEMOCRITOS, Istituto Officina dei Materiali, Consiglio Nazionale delle Ricerche and SISSA Scuola Internazionale di Studi Superiori Avanzati, Via Bonomea 265, I-34136, Trieste, Italy.*

E-mail: fabris@iom.cnr.it

[*]To whom correspondence should be addressed
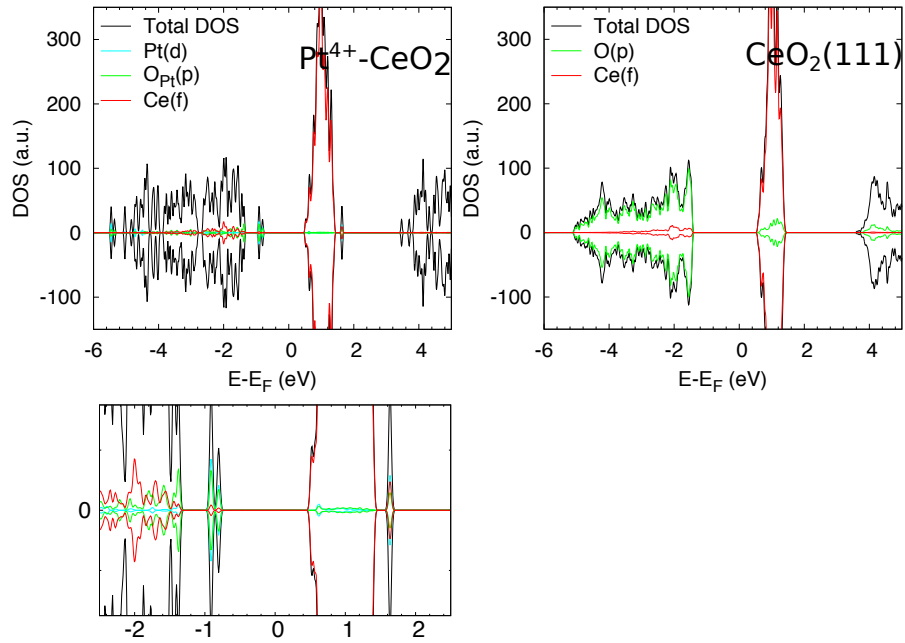
# Contents

# S1   Electronic structure analysis



Figure S1: DOS and PDOS of Pt-CeO$_2$(111) solid solution surface (left panel, its inset is displayed below) and pristine CeO$_2$(111) surface (right panel).
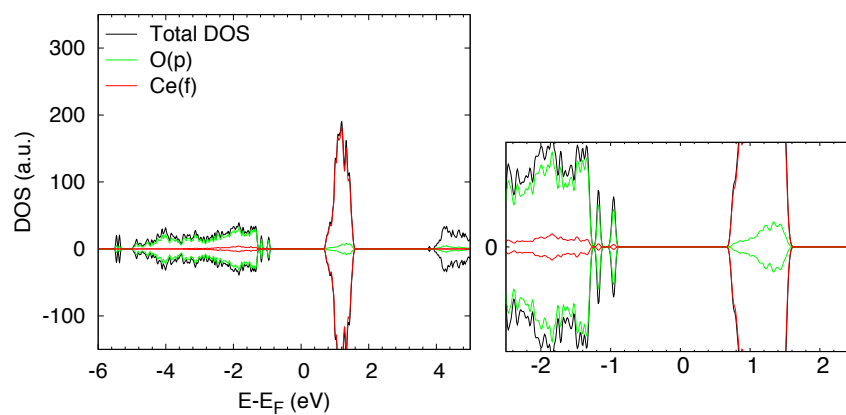
Figure S2: Total DOS and PDOS of methanol dissociation on pristine CeO$_2$(111) surface. The inset around the Fermi level is displayed on the right.
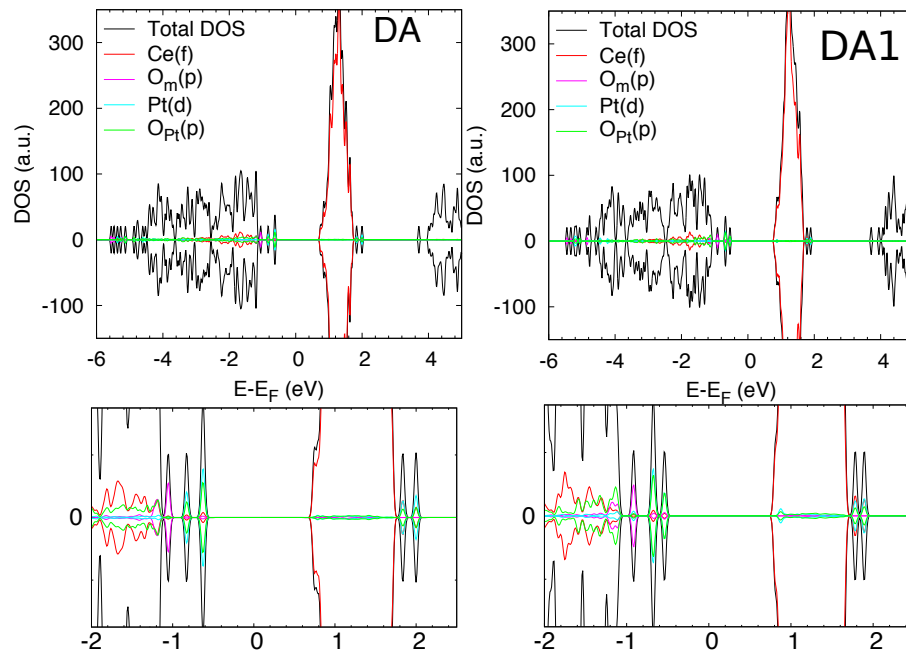
Figure S3: DOS and PDOS of methanol dissociative configurations on Pt-CeO$_2$(111) solid solution surface.

Table S1: Bader Charge analysis of lowest-energy methanol adsorption and dissociation on $CeO_2$ (111) and Pt - $CeO_2$ (111) solid solution surfaces.

|          | $CeO_2(111)$ | | $Pt^{4+}CeO_2(111)$ | |
|----------|-------|-------|-------|-------|
|          | MA    | DA    | MA    | DA    |
| O        | -1.22 | -1.68 | -1.21 | -1.18 |
| H        | +0.64 | +1.00 | +0.73 | +1.00 |
| $O_m$    | -1.40 | -1.42 | -1.49 | -1.40 |
| $O_{Pt}$ | –     | –     | -1.03 | -1.53 |
| Pt       | -     | -     | +1.51 | +1.56 |

# S2 Metastable configurations
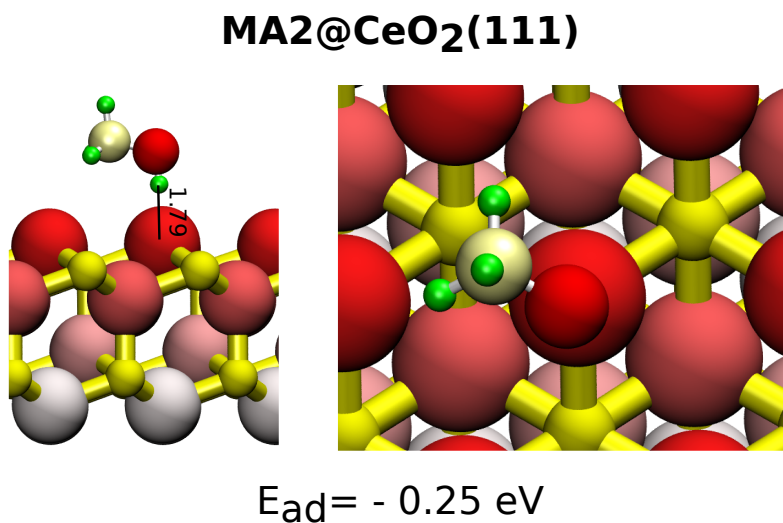
**MA2@CeO$_2$(111)**



$E_{ad}$= - 0.25 eV

Figure S4: Side view (left) and top view (right) of the second lowest energy adsorption configuration of methanol on CeO$_2$(111) surface.
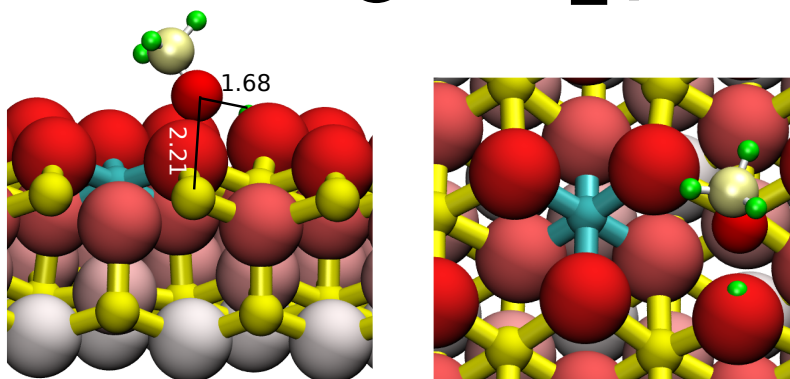
# DA1 Pt$^{4+}$@CeO$_2$(111)



Figure S5: Side view (left) and top view (right) of the dissociative adsorption configuration (DA1) of methanol on Pt$^{4+}$CeO$_2$(111) surface. The O$_m$-H and O$_m$-Ce distances are 1.68 Å, and 2.21 Å, respectively. The adsorption energy E$_{ad}$ is 0.44 eV.

# S3 Adsorption configurations at step-edges



Figure S6: Left panel: molecular adsorptions of methanol on Step I-S (a, c) and $Pt^{2+}$@ Step I-S (e, g). Right panel: dissociative adsorptions of methanol on Step I-S (b, d) and $Pt^{2+}$@-Step I-S (f, h).
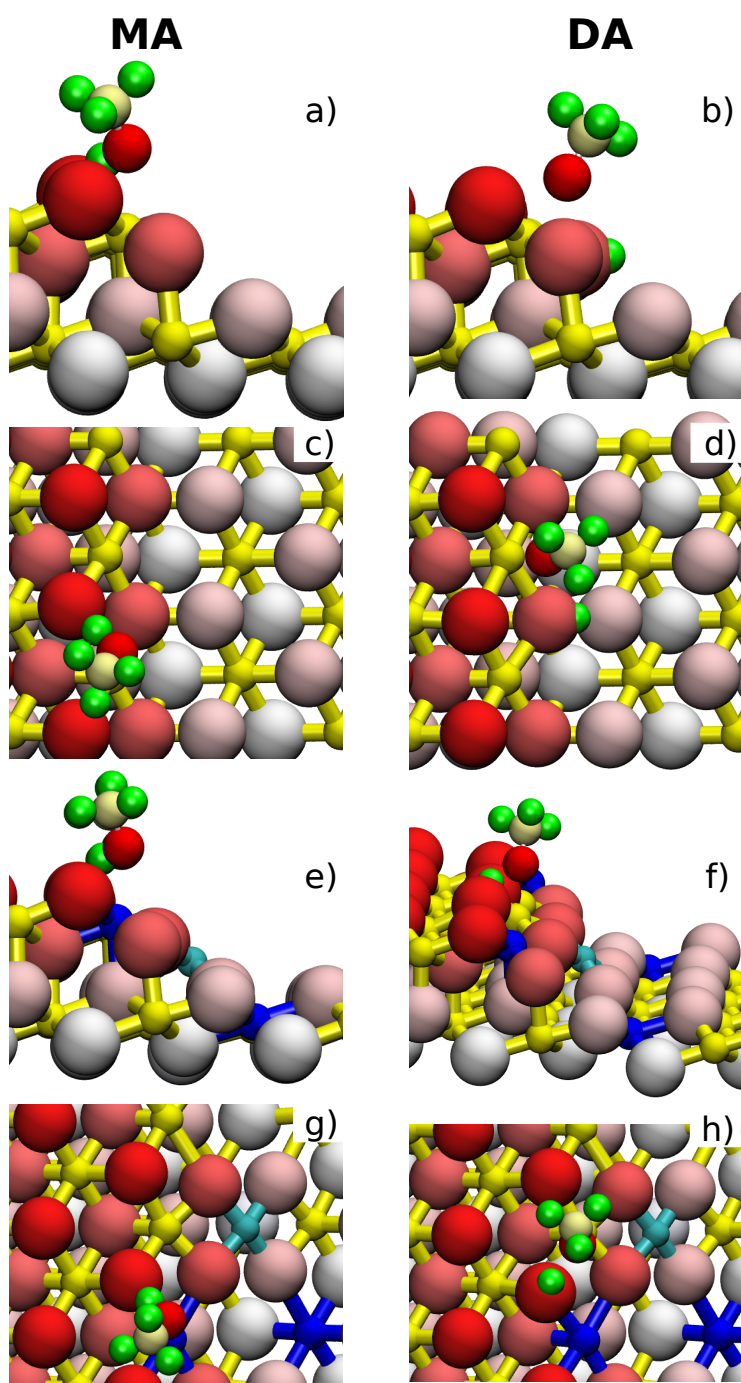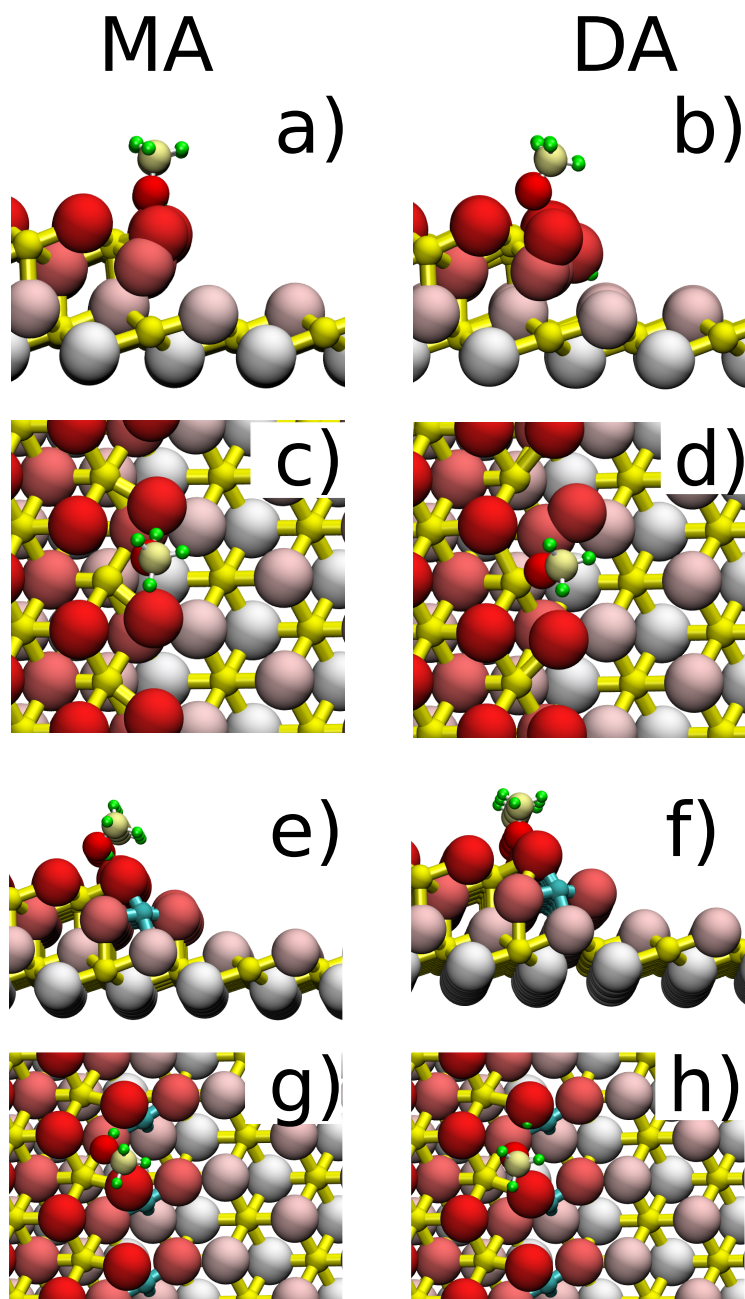
Figure S7: Left panel: molecular adsorptions of methanol on Step I-O (a, c) and $Pt^{2+}$@ Step I-O (e, g). Right panel: dissociative adsorptions of methanol on Step I-O (b, d) and $Pt^{2+}$@-Step I-O (f, h).

# S4 Adsorption configurations at supported cluster
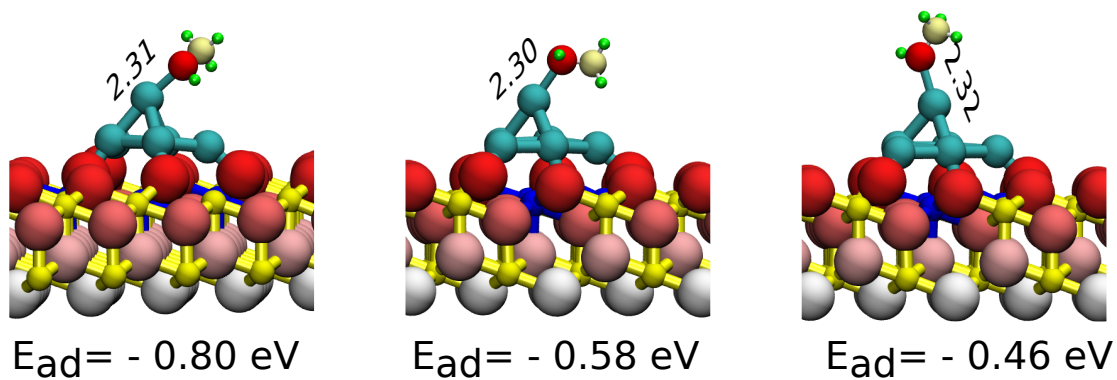


Figure S8: The molecular adsorption configurations (MA) with different rotations of methanol on $Pt_6CeO_2(111)$ surface.
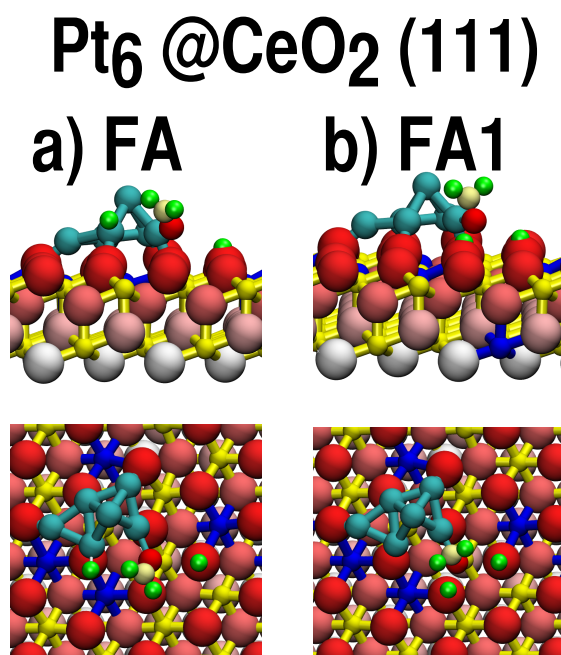
# Pt$_6$ @CeO$_2$ (111)

## a) FA

## b) FA1



Figure S9: The formaldehyde adsorptions (FA) around interfacial Pt site of supported cluster surface.

# S5 Coverage effects and Monkhorst-Pack k-point sampling convergence

Table S2: Methanol adsorption energies (eV) as a function of coverages $\theta$ on $CeO_2$ (111) and Pt - $CeO_2$ (111) solid solution surfaces

|         | $CeO_2(111)$ | | $Pt^{4+}CeO_2(111)$ | | |
|---------|------|------|------|------|--------|
|         | MA   | DA   | DA   | MA   | DA1    |
| 0.25 ML | - 0.53 | - 0.62 | - 1.17 | - 0.48 | - 0.27* |
| 1/9 ML  | - 0.50 | - 0.66 | - 0.98 | - 0.44 | - 0.44 |

*) surface reconstruction occurred

For the lower coverage $\theta = 1/9$ ML, methanol adsorption and dissociation on pure $CeO_2(111)$ surface were computed with a larger supercell, (3x3), and the $\Gamma$-point sampling was used for the integration over the BZ, correspondingly. The final results of adsorption energies are reported in Table S2. It turns out that methanol adsorption energies (MA and DA) are just slightly different with respect to the higher coverage case (0.25 ML), the variation being within 0.05 eV.

On Pt-$CeO_2$ solid solution surface, we also consider the case of coverage $\theta = 0.25$ ML in addition to the 1/9 ML case in the main text. The calculations were performed with (2x2) supercell and (2x2x1) Monkhorst-Pack k-point grid, similar to the corresponding case of pure (111) surface. On this smaller supercell, we still observe the barrierless DA with lower adsorption energy, - 1.17 eV (see Table S2). In summary, the denser coverage does not affect the methanol dissociation prompted by the $Pt^{4+}$ ions. Other higher-energy MA and DA1 metastable configurations have adsorption energies of - 0.48 eV and - 0.27 eV, respectively (see Table S2). Note that there is a surface reconstruction occurred during this methanol dehydrogenation (DA1). This could be result of combinative effects between methanol dehydrogenation at higher coverage and denser density of $Pt^{4+}$ ions. Also note that, at this coverage, methanol dissociation does not reduce the ceria substrate.

Table S3: K-point sampling convergence results for adsorption energies (eV) for some lowest-energy DA configurations selected from the main text.

| | $\Gamma$-point | 2x2x1 | 3x3x1 | 4x4x1 |
|---|---|---|---|---|
| $CeO_2(111)$ | -0.713 | -0.624 | -0.622 | -0.623 |
| $Pt^{4+}@CeO_2(111)$ | - 0.978 | - 0.982 | - 0.978 | – |
| Step I-S | -1.175 | -1.186 | – | – |

Table S3 shows convergence results with respect to Monkhorst-Pack k-point meshes. Some lowest-energy DA configurations on ceria-based surfaces were selected from the main text, including $CeO_2(111)$ ((2x2) supercell), $Pt^{4+}@CeO_2(111)$ ((3x3) supercell), and Step I-S. Their adsorption energies at denser k-point meshes, up to (4x4x1), were re-computed. Comparing to the corresponding adsorption energies reported in the main text, the adsorption energies at denser k-point meshes varies within 0.01 eV.